Eur. Phys. J. B **37**, 405–411 (2004)
DOI: 10.1140/epjb/e2004-00073-5

THE EUROPEAN PHYSICAL JOURNAL B

LDA and GGA investigations of some ground state properties of aluminium with the all electron MAPW method

H. Bross[a]

Sektion Physik Universität München, Theresienstr. 37IV, 80333 München, Germany

Received 17 November 2003
Published online 2 April 2004 –

Abstract. Both in local-density approximation (LDA) and in generalised-gradient approximation (GGA) the electronic structure of Aluminium is evaluated by use of the modified augmented plane wave (MAPW) self-consistent scheme. The LDA based on the exchange correlation functional by Vosko, Wilk and Nusair gives the equilibrium lattice constant in good accord with its experimental value. The hole sheet of the Fermi surface, h_2, is well described by weakly distorted spheres with origin at $(2,0,0)\frac{2\pi}{a}$ and $(1,1,1)\frac{2\pi}{a}$ in the reciprocal lattice. Near and above the equilibrium lattice constant the electronic sheet, e_3, is found to be quite similar to the model originally proposed by Ashcroft. However, even moderate compressions induce a drastic variation.

PACS. 71.18.+y Fermi surface: calculations and measurements; effective mass, g factor – 71.20.-b Electron density of states and band structure of crystalline solids

1 Introduction

In the past the electronic structure of Aluminium, especially the shape of the Fermi surface (FS) has been extensively investigated, mostly by use of the pseudopotential method. By comparing with de Haas-van Alphen (dHvA) experiments Ashcroft [1] proposed the electronic sheet e_3 to consist of four spindles connected at the edges of the square faces of the fcc Brillouin zone (BZ). In this model the state $W_2^{'}$ is not occupied in contrast to the competing model [2] where the four spindles are joined near each W-point. In the following decades the first model was confirmed by high-precision dHvA experiments [3–5] supported by pseudopotential calculations [1,4–6] with suitably chosen potential Fourier coefficients or Korringa-Kohn-Rostocker (KKR) calculations [7] with suitably chosen phase shifts, both allowing a consistent description of the experimental data. Although the shape of the FS is, with some reservation as for example the total energy, the charge density, or the Fermi energy, a ground state property in the case of Al no sophisticated investigation has been performed using the self-consistent potential obtained by modern LDA or GGA investigations and highly accurate band structure schemes. The present investigation closes this gap. Section 2 reports on results from all-electron MAPW calculations using various exchange-correlation functionals in LDA and GGA. Similar to a previous investigation [8] the LDA functional by Vosko, Wilk and Nusair [9] produces an equilibrium lattice constant in closer agreement with the experimental value than the GGA. In Section 3 it is found that important details like the position of the state $W_2^{'}$ relative to the Fermi level are quite sensitive to the lattice constant with the consequence that even a small compression of the lattice significantly varies the shape of the electronic FS sheet.

[a] e-mail: helmut.bross@cm.physik.uni-muenchen.de

2 Evaluation of the electronic structure

2.1 The all-electron MAPW-scheme

The band structure problem was solved within the all-electron self-consistent MAPW framework in LDA and GGA. As remarked by Boettger and Trickey [10] in the GGA special care is advisable as it also needs the gradient and the Laplacian of the charge density. In contrast to previous investigations [11–14] where most of the details of the scheme are described we do not use the quadratic $r-$mesh originally proposed by Moruzzi et al. [15] but define the radial points by

$$r_i = r_0 * \left[1 - \cos\frac{\pi}{2}\frac{i-1}{i_0-1}\right] \qquad 0 \le i \le i_0 \tag{1}$$

$$r_i = r_0 * \left[1 + \frac{\pi}{2}\frac{i-i_0}{i_0-1}\right] \qquad i_0 \le i \le i_{apw} \tag{2}$$

$$\text{where} \quad r_0 = r_{apw} / \left[1 + \frac{\pi}{2}\frac{i_{apw}-i_0}{i_0-1}\right], \tag{3}$$

which is more appropriate in the valence electron region. Suitably the integers i_0 and i_{apw} are chosen to be 120

and 160, respectively. The MAPW scheme allows to treat the core electrons in the same way as the valence electrons i.e. the Bloch-functions are approximated by a superposition of plane waves augmented inside the APW-sphere by a product of spherical harmonics and properly chosen radial functions. In contrast to the generic augmented plane wave APW-scheme we can restrict the angular quantum number for the s-p-metal Al to 2 since additional constraints make the wave functions continuously differentiable at the surface of the APW-sphere. All occupied electronic states are converged to 1 mRyd by considering approximately 50 plane waves and 5 different radial functions for each value of the angular momentum $\mathrm{l} \leq 2$. From the occupied states the electronic density $n(\boldsymbol{r})$ is then determined. As a consequence of the MAPW ansatz a symmetric combination of plane waves superimposed by an angular dependent contribution within the APW sphere is obtained. To avoid any truncation error the latter contribution was evaluated along 6 different directions specifically chosen [16–20] in the 1/48th of the unit sphere. By averaging over all angular dependent contributions from these directions the crystal potential of warped muffin-tin shape in LDA is found. In GGA the charge density along these directions is fitted to a sum of products of spherical harmonics $r^l Y_{lm}(\boldsymbol{r}^0)$ and radial functions $\rho_l(r)$. This has the advantage that $\nabla\, r^l Y_{lm}(\boldsymbol{r}^0)$ is a superposition of spherical harmonics of order $(l-1)$ and that the Laplacian of the spherical harmonics vanishes. The radial derivative of $\rho_l(r)$is obtained from the cubic spline interpolant of $\rho_l(r)$. This procedure is numerically reliable since its derivatives at $r = 0$ and $r = r_{apw}$ are known with high accuracy. The radial part of the Laplacian is found by spline interpolation of the function

$$f(r) = r^2 \frac{d\rho_l(r)}{dr}, \qquad \text{hence} \tag{4}$$

$$\frac{d^2\rho_l}{dr^2} + \frac{2}{r}\frac{d\rho_l}{dr} = \frac{1}{r^2}\frac{df}{dr}. \tag{5}$$

Both steps guarantee that the input for the *GGA* is sufficiently accurate. Outside the APW sphere a suitably chosen fine mesh of equidistantly distributed $\boldsymbol{r}$-points allows to treat exchange and correlations contributions in LDA and GGA to any accuracy wanted. In the LDA scheme exchange and correlation are described by a functional proposed by Vosko et al. [9] which in the case of Lithium brought the lattice constant quite close to its experimental value [14]. The GGA functionals proposed by Perdew et al. [21] and by Perdew et al. [22] are used, which in the following are denoted by *pw91* and *pbe*, respectively. By neglecting the local variation of the density $n(\boldsymbol{r})$ in the GGA-functionals e.g. setting $\nabla n(\boldsymbol{r})$ and $\Delta n(\boldsymbol{r})$ equal zero additional LDA results are obtained, denoted by $pbe = 0$. Finally the BZ integrations over the occupied states yielding the electron density and the total energy are approximated by sums over a varying numbers of properly chosen $\boldsymbol{k}$ points in the irreducible wedge [23–25]. Not only in the use of this more elaborate functional but in the warped muffin-tin approximation of the crystal potential and the numerical accuracy guaranteed by the choice of some intrinsic parameters the present work differs from other investigations.

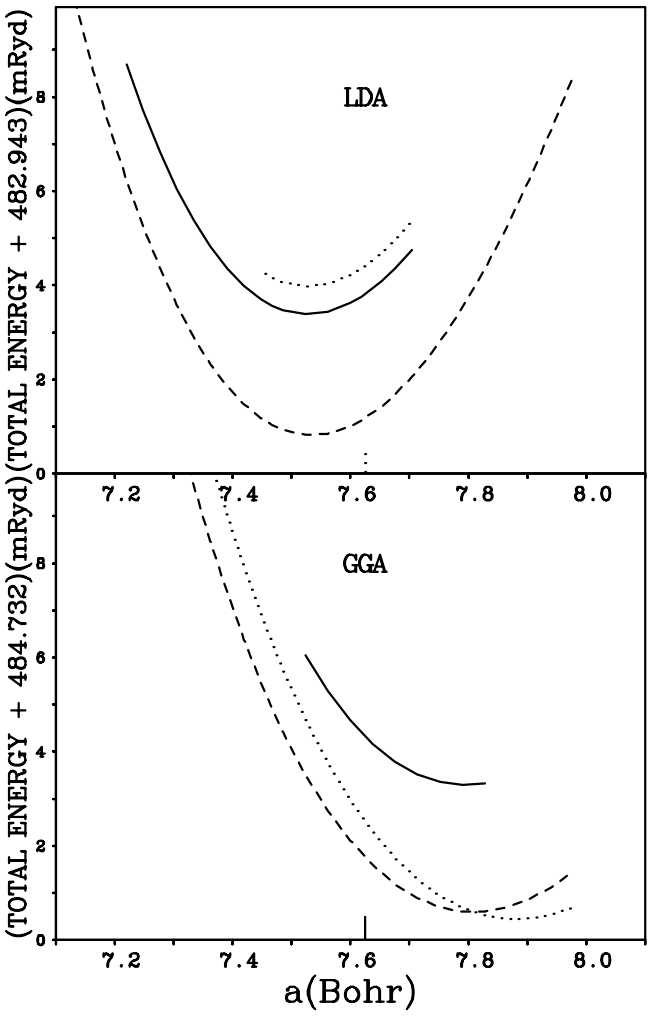

Fig. 1. Dependence of the total energy E_{tot} relative to certain offsets on the lattice constant a. Upper panel: LDA results: Dashed line 110, full line 770, dotted line: 5740 $\boldsymbol{k}$-points, respectively. Lower panel: GGA-*pbe* results: Dashed line 110, full line 770 $\boldsymbol{k}$-points, respectively and GGA-*pw91* results with offset −484.966 Ryd: Dotted line 110 $\boldsymbol{k}$-points.

2.2 Results of the total energy calculations, GGA versus LDA

Self-consistent calculations both in LDA and in GGA were performed at equally spaced values of the lattice constant in the interval $[6.992, 7.980]$ a.u. The result of all calculations with various grids of $\boldsymbol{k}$-points are summarised in Figure 1 which shows the total energy as function of the lattice constant after a shift by an appropriately chosen offset. In the upper panel the LDA-*vwn* results are displayed obtained by considering 110, 770 and 5740 $\boldsymbol{k}$-points in the irreducible wedge. These curves differ from each other by rigid vertical shifts of 2.6 mRyd and 0.6 mRyd, respectively but give consistent values of the curvature.

Table 1. Ground state magnitudes for different exchange correlation functionals. *hl*: LDA functionals according Hedin and Lundqvist [26]. *vwn*: LDA functionals according Vosko et al. [9]. *pbe* = 0: GGA functionals according Perdew, Burke and Ernzerhof [22] but local variation of the potential neglected. *pbe*: GGA functionals according Perdew, Burke and Ernzerhof [22]. *lda-pbe*: as pbe but using the LDA-*vwn* density. *pw91*: GGA functionals according Perdew et al. [21].

	a_0(Bohr)	$E_{tot,0}$(Ryd)	B(GPa)	$\frac{dB}{dp}$	γ
hl	7.4736	−483.38905	89.45	4.91	3.728
vwn	7.5347	−482.94218	80.34	5.08	3.754
pbe = 0	7.5371	−482.93312	80.08	5.02	3.767
pbe	7.8091	−484.73146	53.23	3.39	4.330
lda − *pbe*	7.8110	−484.72660	55.09	3.20	4.273
*pw*91	7.8811	−484.96556	46.65	4.10	4.281
exp	7.6194		81.97	3.9	

From these results we learn that with respect to the position of the minimum and the curvature of the E_{tot}-curve in LDA a mesh of 110 points is only just sufficient. In the lower panel the GGA results obtained with the functionals [21,22] are plotted. With respect to the position of the minimum and the curvature of the energy curve all GGA results are quite similar; varying the $\boldsymbol{k}$-grids and using different functionals only has an effect on the magnitude of the energy offset. However, by comparing both panels we must conclude that the GGA scheme based on the cited functionals reduces the interatomic forces with the consequence that a bigger value of the lattice constant is predicted and the curvature of the energy curve is reduced.

To make this more quantitative, for each set of lattice constants the total energy has been interpolated by a cubic spline. The characteristic values of this local fit, e.g. the total energy $E_{tot,0}$, the lattice constant a_0 and the isothermal bulk modulus B at the minimum, are listed in Table 1. In addition the value of the pressure derivative of the bulk modulus is also given which is found by the Legendre transform with the independent variable p and the enthalpy-like function

$$H(p) = E_{tot} + pV, \quad p = -\frac{dE_{tot}}{dV} \tag{6}$$

yielding

$$\frac{dB}{dp} = V_0 \frac{d^3H}{dp^3} / \frac{d^2H}{dp^2} - 1, \tag{7}$$

where V_0 is the volume of the atomic cell at zero pressure. Finally by a proper choice of the parameter γ the volume dependence of the total energy has been globally fitted to the Murnagham equation [14,27]

$$E_{tot} = E_{tot,0} - \frac{BV_0}{\gamma - 1} + \frac{BV}{\gamma}\left[\frac{1}{(\gamma-1)}\left(\frac{V_0}{V}\right)^{\gamma} + 1\right]. \tag{8}$$

In the last row of Table 1 experimental values are given. The lattice constant a was obtained by Coleridge and Holtham [5] by extrapolating the 20.4 K measurements by Figgins et al. [33] to zero temperature. The bulk modulus is given by

$$B = \frac{c_{11} + 2c_{12}}{3}, \tag{9}$$

where the elastic constants c_{11}, c_{12} are taken from ultrasonic experiments at $T = 4$ K [28]. $\frac{dB}{dp}$ is a mean value of different measurements according to [29].

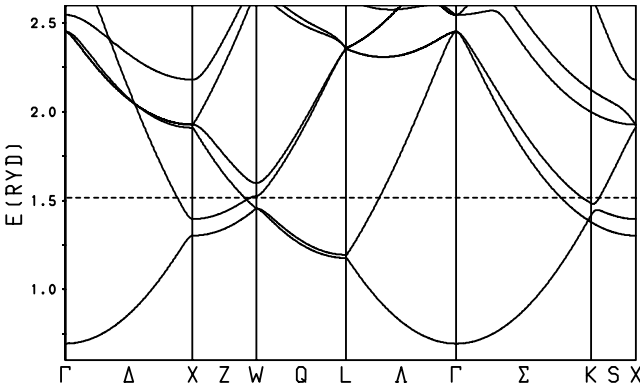

Fig. 2. Band structure of fcc Al along the major symmetry directions for the lattice constant $a = 7.6190$ a.u. The horizontal line marks the Fermi level at $E_F = 1.5080$ Ryd.

The comparison surprisingly shows that the *LDA* investigations with the functionals [9] improve the agreement with the experimental values of the lattice constant whereas the bulk modulus is still too small. Both *GGA*-investigations overestimate the lattice constant considerably and give a a still smaller value of the bulk modulus. The functionals denoted by *pbe* are definitely superior to the functionals *pw*91 as they bring the lattice constant closer to the experimental value. These findings stand in contrast to previous investigations which for lighter elements favour the functionals *pw*91 [8,30,31]. However, a glance at Table III compiled by Boettger and Trickey [10] reveals that there is no clear trend in the lattice constants and bulk moduli calculated with diverse approximations. Especially in GGA it is likely that the scatter in the results reflects a high sensitivity to the numerical precision of the density-gradient evaluation.

As a further consistency check of our *GGA* results we have also calculated the total energy by use of the self-consistent charge density of our *LDA* calculations. Thus the influence of the exchange and correlation functionals which strongly depend on the second derivative of the charge density and for example produce an additional singularity at the nuclei are completely excluded. It is quite remarkable that this alternative evaluation causes only an almost rigid, vertical shift of the total energy by 5 mRyd without any change of the shape of the energy curve.

3 Fermi energy, density of states and some features of the Fermi surface

In Figure 2 the LDA band structure of fcc Al for $a = 7.619028$ a.u. = 4.0318 Å, which is quite close to the experimental value [5] is displayed. Its overall features are

Table 2. The width W of the occupied valence bands, the energy E_W of the state $W_2^{'}$ relative to the Fermi energy, the density of the states at the Fermi energy. First line: LDA-vwn result, second line: GGA-pbe result, respectively.

a[a.u.]	7.2200	7.4480	7.5240	7.6000	7.6190	7.6526	7.6760
W[Ryd]	0.9043	0.8540	0.8381	0.8225	0.8187	0.8119	
			0.8408	0.8251			0.8098
E_W[mRyd]	−14.6	−5.1	3.4	8.1	9.2	11.0	
			0.4	4.8			9.3
$N(E_{\rm F})/N^0(E_{\rm F}^0)$	1.5464	1.5646	1.5468	1.5417	1.5411	1.5337	
			1.5512	1.5368			1.5330

Table 3. Cross-sectional areas and cyclotron mass of the orbits ψ[100], ψ[110] and ψ[111] as function of the lattice parameters. Last column: Experimental results. [a] Coleridge and Holtham [5], [b] Anderson and Lane [4], [c] Moore and Spong [38]. Areas in units of $(\frac{2\pi}{a})^2$, cyclotron masses in units of the free-electron mass.

a[a.u.]	7.2200	7.4480	7.5240	7.6000	7.6190	7.6526	7.6760	
ψ_{100}	2.5524	2.5786	2.5881	2.5975	2.5998	2.6039	2.6069	2.66 ± 0.08^b
ψ_{110}	1.6881	1.6940	1.6958	1.6975	1.6979	1.6986	1.6991	1.695 ± 0.003^a
ψ_{111}	1.6181	1.6249	1.6274	1.6301	1.6308	1.6320	1.6329	1.621 ± 0.003^a
$\lvert m_c[100]\rvert$	1.7736	1.8887	1.9146	1.9408	1.9475	1.9592	1.9602	1.30 ± 0.1^b, 1.27^c
$\lvert m_c[110]\rvert$	1.0430	1.0672	1.0753	1.0835	1.0855	1.0891	1.0916	
$\lvert m_c[111]\rvert$	1.1421	1.1689	1.1785	1.1885	1.1910	1.1957	1.1988	1.36 ± 0.1^b, 1.40^c

rather similar to other investigations compiled in reference [32], especially for the lowest valence bands. At the W-point we find the state $W_2^{'}$ definitely above the Fermi level which, as we shall see, significantly influences the shape of the electron sheet e_3. The width W of the occupied valence bands, the energy E_W of the state $W_2^{'}$ relative to the Fermi energy E_F, the density of states at the Fermi energy $N(E_F)$ divided by its value in the case of the homogeneous electron gas of the same density are listed in Table 2 for different lattice constants. These values are obtained either by LDA with the functionals [9] or by GGA with the functionals [21,22] using 770 $\boldsymbol{k}$-points in the irreducible wedge. Especially the energy of the state $W_2^{'}$ turns out to sensitively depend on the lattice constant: at $a = 7.4568$ a.u. it crosses the Fermi level inducing a drastic change of the sheet e_3. By considering denser integration grids in the BZ we have checked that these results are almost converged, for example in the case of 4218 points $E_{W_2^{'}}$ coincides with E_F at $a = 7.4624$ a.u.

In contrast to the energetics treated in the last section the GGA based on the functionals [21] and [22] has minor influence on the band structure: the energy $W_2^{'}$ state crosses the Fermi level at $a = 7.5126$ a.u. and $a = 7.40784$ a.u., respectively. But due to the smaller value of the bulk modulus a higher compression relative to the minimum of the total energy is needed to induce the characteristic change of the sheet e_3. Experiments at low temperature are best described by the fifth column of Table 2 which corresponds to $a = 4.0318$ Å [33]. The density of states determined from the low-temperature electronic specific heat [34] is about 1.6 times the free electron value. Compared to other metals the mass enhancement caused by the electron-phonon interaction [35,36] turns out to be rather small.

The present investigation confirms the old concept that in the extended zone scheme the FS of non-compressed Al is approximately described by spheres with origins at the lattice vectors $\boldsymbol{K}$ and with radius determined by 3 electrons in the atomic cell, $k_F = (\frac{9}{2\pi})^{1/3}\frac{2\pi}{a}$. The crystal potential only induces non-marginal changes near the surface of the BZ. Thus the dominant sheet of the FS within the first BZ is a truncated octahedron at the point Γ which is denoted by h_2 as it mainly consists of hole states (see for example Cracknell [37]). With respect to its shape all previous investigations [1,3–6] arrived at a similar result. We have found that in the extended zone scheme spheres located at next nearest lattice vectors which are stretched in the $[1,0,0]$ direction by 0.93% and compressed by 0.67% in the $[1,1,0]$ and in the $[1,1,1]$ direction are close to the sheet h_2 apart from the neighbourhood of the Brillouin zones. Within the first BZ the sheet h_2 is closed and mostly consists of 12 spherical caps with centres at the points $(1,1,1)\frac{2\pi}{a}$ and $(2,0,0)\frac{2\pi}{a}$. Consequently the intersections of the FS with central planes having normals in the directions of high symmetry, commonly denoted by ψ[100], ψ[110] and ψ[111], consist of circular arcs which are more or less rounded at the locations of their intersections. However, the intersection ψ[100] has a sharp cusp which is caused by the accidental degeneracy with the third-zone FS in the plane (1,0,0) near the point W. The orbits ψ[100], ψ[110], and ψ[111] have been extensively investigated by the dHvA effect and by cyclotron resonance, see for example [4,5,38]. In Table 3 the cross-sectional areas A and the cyclotron masses m_c obtained by our first-principles calculations are compared with

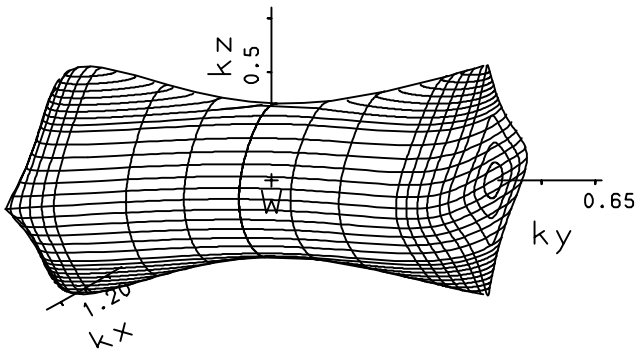

Fig. 3. Element of the FS e_3 of Al($a = 7.22$ a.u.). The right half originates from rotation by π along the line [1,0,1] through the point W. In k_z-direction the scale is enlarged by a factor of 10.

different experimental results. For all three orbits a quite close agreement is found. In contrast to a previous pseudopotential investigation [4] based on three heuristic parameters in [110]- and [111]-direction the cyclotron masses satisfactorily agree with the experimental results. Obviously the MAPW-calculations lead to a stronger variation of the Fermi calibres with energy than the pseudopotential scheme. The remaining differences can be ascribed to electron-phonon interaction but are distinctly smaller than those predicted by Ashcroft and Wilkins [35]. The larger values of m_c [100] are caused by the degeneracy with the electronic sheet which considerably enhances the energy derivative $\frac{dk_F}{dE}$ at certain points of the ψ[100]-orbit.

The other sheet of the FS, e_3, is quite sensitive to the crystal potential as it is essentially located near the surface of the BZ. According to Table 2 small compressions shift the state $W_2^{'}$ below the Fermi level which has drastic consequences on the shape of e_3. From our investigations at different values of the lattice parameter we learn that it is formed by a combination of two types of basic elements which at moderate compression $a/a_0 \leq 0.98$ do not interact: the spindle and the dumb-bell. The spindle has the shape of a prolate ellipsoid with the major axis along the edge of a square face of the BZ and the centre near a point U. As a possible type of the FS spindles already have been mentioned by Ashcroft ([1], Fig. 9) who called them "arms". With decrease of the compression the spindle is uniformly stretched. The dumb-bell near the point W$(1,\frac{1}{2},0)$ is almost rotational-symmetric along the k_y direction through this point as shown in Figure 3. It is hard to imagine how such a geometrical element might be composed of spherical caps which are the reminiscence of the pseudopotential scheme. This is likely the reason why Ashcroft [1] and other pseudopotential investigations did not find this element. The shape of the dumb-bell sensitively depends on the lattice parameter. In k_y direction it remains restricted to the domain $[0.42, 0.58]$ a.u. Its maximum extension perpendicular to the k_y-axis increases with the relaxation of the lattice whereas its neck drastically shrinks and approaches the value zero at $a = 7.456$ a.u. with the consequence that the dumb-bell splits into two parts.

This different behaviour of the spindles and the dumb-bells has a crucial influence on the shape of e_3 and its extremal cross- sections. Below $a = 7.354$ a.u. well-separated spindles and dumb-bells form the FS with closed orbits only. They are denoted either by γ or by β following the notation [4]. At $a = 7.354$ a.u. the neighboured spindles and dumb-bells come into contact. Then e_3 becomes multiply connected and extends continuously throughout $\boldsymbol{k}$-space. In a magnetic field both unbounded and closed orbits are possible and consequently the magnetoresistance will only show saturation at certain orientation of the magnetic field. On the joint of a spindle and a dumb-bell a new type of minimal orbit denoted by α appears which already has been suggested by Ashcroft [1][1]. A further orbit denoted ξ runs on the intersection of the squared face with the four spindles. No evidence has been found for the existence of an extremal orbit around the junction of the four spindles with the dumb-bell of the type proposed by Harrison [2]. Above $a = 7.448$ a.u. the FS is no longer multiply connected because the dumb-bells split up. In accordance with the proposal by Larson and Gordon [4] based on a refined analysis of the experimental data the four spindles on the edges of the square face of the BZ are connected by one-half of a dumb-bell originally located at the corner of the square face. These considerations are supported by Table 4 which lists a choice of extremal cross sections mostly centred near the points W$(1,\frac{1}{2},0)$ and U$(1,\frac{1}{4},\frac{1}{4})$[2].

Orbits of type α and ξ occur only after the merging of the spindles and the dumb-bells. The minimal orbits $\beta^{'}$ on the dumb-bells decrease with increasing lattice parameter and approach the value zero at $a = 7.456$ a.u. when the dumb-bells split up. Almost all other orbits grow with increasing lattice parameter. In the final column experimental results obtained by dHvA experiments [5] are listed which are close to previous results [3,4]. The agreement with our first-principles results is satisfying but not as good as with those derived with the pseudopotential based on three heuristic parameters [4–6]. Certainly part of the differences are due to the fact that the Kohn-Sham FS determined in the present investigation not fully incorporates many-body effects [40].

One aspect warrants further discussion. For the magnetic field along the [100] direction there is an accidental degeneracy between the second zone ψ-orbit and the third zone α-orbit which considerably enhances the cyclotron masses. This degeneracy is raised only by spin-orbit effects which, being small in Al, cause a small energy gap. As it is easily broken down by a magnetic field the corresponding dHvA oscillations are weak and difficult to observe [5].

[1] Similar as in the case of the experiments it was not possible to uniquely resolve some α and β orbits.

[2] Great care has been taken to localise the exact position of every orbit by finding the extremal value of the corresponding area.

Table 4. Cross-sectional areas of e_3 enlarged by the factor 100 in units of $(\frac{2\pi}{a})^2$. Last column experimental results by dHvA experiments [5]. Minimum orbits are denoted by a †. The corresonding values of the centres of the orbits and of the cyclotron masses are available in electronic form.

a[a.u.]		7.2200	7.296	7.372	7.4480	7.5240	7.6000	7.6190	7.6194
α[001]	†			0.0142	0.0690	0.1198	0.1309	0.1340	0.1110±0.0004
α[001]						0.3035	0.2219	0.2063	0.1839±0.0012
α[010]						0.0701	0.0835	0.0869	
α'[010]	†				0.1488	0.2611	0.3630	0.3866	
$\alpha[0\bar{1}1]$	†			0.0115	0.0574	0.0932	0.1186	0.1233	0.1026±0.0004
α[101]	†					0.3053	0.2378	0.2258	0.1992±0.0008
$\alpha[10\bar{1}]$				0.0259	0.1304	0.2251	0.2361	0.2259	
$\alpha[11\bar{1}]$	†			0.0152	0.0772	0.1272	0.1685	0.1759	
α[111]						0.1272	0.1669	0.1758	
β[001]		1.7409	1.5414	1.3439					
β[010]		0.6609	0.6053	0.5704	0.5942	0.7007	0.8348	0.8689	
β'[010]	†	0.3623	0.2403	0.1228	0.0122				
β[011]		0.7086	0.5971	0.5018					
β'[011]	†	0.5723	0.3855	0.1998	0.0201				
β[110]		0.7383	0.6234	0.5311					
$\beta[\bar{1}01]$		1.5402	1.3522	1.1430	0.8836				
β[111]		0.8451	0.6926	0.5786	0.2477				
β'[111]	†	0.7872	0.5461	0.2934	0.0307				
γ[001]		0.5325	0.7702	0.9987	1.2192	1.4308	1.6310	1.6789	1.5378±0.0004
γ[100]		1.8336	2.6295						
γ[100]		1.8401	2.6391						
γ[011]		1.6799	2.3469	2.8367					
$\gamma[01\bar{1}]$		0.3898	0.5654	0.7349	0.8992	1.1669	1.2082	1.2443	1.1371±0.0004
γ[101]		0.7116	1.0262	1.3268	1.6343	1.8916	2.1775	2.2146	
γ[111]		1.6540	2.3893	3.0998	3.7953	4.4502	5.1437	5.2329	
$\gamma[11\bar{1}]$		0.4713	0.6826	0.8858	1.1083	1.2738	1.4539	1.4971	1.3716±0.0012
ξ[100]				37.240	36.317	35.657	35.173	35.075	34.69±0.06
ζ[100]				37.240	36.317	35.657	35.173	35.075	15.24±1.57

4 Concluding remarks

A very dense grid of $\boldsymbol{k}$-points is required to properly resolve the contribution of the sheet e_3 to the value of the Fermi energy, the density $n(\boldsymbol{r})$, etc. Most of the previous investigations do not satisfy this requirement. As most of the extremal areas of e_3 are found to be quite sensitive to the lattice constant it makes no great sense to determine the derivative of these magnitudes with respect to the pressure as has been done in a previous investigation [39].

The author would like to thank PD Dr. Engel, Universität Frankfurt, for providing his DF codes and for enlightening discussions about the density functional aspect and Dr. R. Bader, LRZ Munich, for extensive advice concerning the numerical work and for critical reading the manuscript. Also thanks for support in producing the figures is due to Mrs. J. Dreer, LRZ Munich.

References

1. N.W. Ashcroft, Phil. Mag. **8**, 2055 (1963)
2. W.A. Harrison, Phys. Rev. **118**, 1182 (1960)
3. C.O. Larson, W.L. Gordon, Phys. Rev. **156**, 703 (1967)
4. J.R. Anderson, S.S. Lane, Phys. Rev. B **2**, 298 (1970)
5. P.T. Coleridge, P.M. Holtham, J. Phys. F **7**, 1891 (1977)
6. W. Joss, R. Monnier, J. Phys. F **10**, 9 (1980)
7. P.T. Coleridge, J. Phys. F **12**, 2563 (1982)
8. A. Khein, D.J. Singh, C.J. Umrigar, Phys. Rev. B **51**, 4105 (1995)
9. S.H. Vosko, L. Wilk, M. Nusair, Can. J. Phys. **58**, 1200 (1980)

10. J.C. Boettger, S.B. Trickey, Phys. Rev. B **51**, 15623 (1995); J.C. Boettger, S.B. Trickey, Phys. Rev. B **53**, 3007 (1996)
11. H. Bross, G. Bohn, G. Meister, W. Schubö, H. Stöhr, Phys. Rev. B **2**, 3098 (1970)
12. H. Bross, R. Eder, Phys. Stat. Solidi (b) **144**, 175 (1987)
13. H. Bross, R. Stryczek, Phys. Stat. Solidi (b) **144**, 675 (1987)
14. H. Bross, Phys. Stat. Solidi (b) **229**, 1359 (2002)
15. V.L. Moruzzi, J.F. Janak, A.R. Williams, *Calculated Electronic Properties of Metals* (Pergamon Press, New York-Toronto-Sydney-Frankfurt-Paris, 1978)
16. A. Bansil, Solid State Commun. **16**, 885 (1975)
17. W.R. Fehlner, S.H. Vosko, Can. J. Phys. **54**, 2159 (1976)
18. W.R. Fehlner, S.B. Nickerson, S.H. Vosko, Solid State Commun. **19**, 83 (1976)
19. R. Prasad, A. Bansil, Phys. Rev. B **21**, 496 (1980)
20. H. Bross, unpublished results
21. J.P. Perdew, in *Electronic Structure of Solids 91* edited by P. Ziesche, H. Eschrig (Akademie-Verlag, Berlin, 1991)
22. J.P. Perdew, K. Burke, E. Ernzerhof, Phys. Rev. Lett. **77**, 3865 (1996)
23. D.J. Chadi, M.L. Cohen, Phys. Rev. B **8**, 5747 (1973)
24. H.J. Monkhorst, J.D. Pack, Phys. Rev. **13**, 5188 (1976)
25. H. Bross, J. Phys. F **8**, 2631 (1978)
26. L. Hedin, B.I. Lundqvist, J. Phys. C **4**, 2064 (1971)
27. F.D. Murnagham, Proc. Natl. Acad. Sci. USA **30**, 244 (1944); J.C. Boettger, S.B. Trickey, Phys. Rev. B **32**, 3391 (1985)
28. J. Vallin, M. Mongy, K. Salma, O. Beckman, J. Appl. Phys. **35**, 1825 (1964)
29. A. Seeger, O. Buck, Z. Naturforsch. a **15**, 1056 (1960)
30. J.P. Perdew, J.A. Chevary, S.H. Vosko, K.A. Jackson, M.R. Pederson, D.J. Singh, C. Fiolhais, Phys. Rev. B **46**, 6671 (1992)
31. S. Kurth, J. Perdew, P. Blaha, Inter. J. Quantum Chem. **75**, 889 (1999)
32. *Landolt-Börnstein*, Volume 13c (Springer Berlin, Heidelberg, New York, Tokyo, 1984), p. 36
33. B.F. Figgins, G.O. Jones, D.P. Riley, Phil. Mag. **1**, 747 (1956)
34. J.G. Daunt in *Progress in Low Temperature Physics* edited by C.J. Gorter (North-Holland Publishing Company Amsterdam, 1964), Vol. 1, p. 210
35. N.W. Ashcroft, J.W. Wilkins, Phys. Lett. **14**, 285 (1965)
36. G. Grimvall, Phys. Kondens. Materie **6**, 15 (1967)
37. *Landolt-Börnstein*, Volume 13c (Springer Berlin, Heidelberg, New York, 1984), p. 39
38. T.W. Moore, F. Spong, Phys. Rev. **125**, 846 (1962)
39. R. Griessen, R.S. Sorbello, Phys. Rev. B **6**, 2198 (1972)
40. D. Mearns, Phys. Rev. B **38**, 5906 (1988)